RSC Mechanochemistry

ROYAL SOCIETY OF CHEMISTRY

PAPER

View Article Online
View Journal | View Issue

Cite this: *RSC Mechanochem.*, 2024, **1**, 393

Advancing sustainable practices in Li-ion battery cathode material recycling: mechanochemical optimisation for magnetic cobalt recovery†

Joshua Vauloup,[a] Cécile Bouilhac,[a] Nicolas Coppey,[c] Patrick Lacroix-Desmazes,[a] Bernard Fraisse,[a] Lorenzo Stievano,[ab] Laure Monconduit *[ab] and Moulay Tahar Sougrati *[ab]

Lithium-ion batteries (LIBs) stand as the dominant power source for electric vehicles owing to their mature technology and exceptional performance. Consequently, metallic components of LIB cathode materials (Ni, Co, Li, and Mn) are assuming strategic significance. The imperative recycling of these metals has necessitated the development of novel technologies that can curtail secondary pollution arising from prevailing hydrometallurgical procedures, including issues such as wastewater generation and excessive energy and chemical consumption. In this study, we present an optimised mechanochemical process tailored for the magnetic recovery of cobalt from $LiCoO_2$, which is a crucial component of LIBs. Our methodology involves the initial reduction of cobalt, facilitated by aluminium, followed by a selective extraction process that leverages the magnetic properties of the obtained species. A systematic exploration of milling parameters was undertaken to comprehensively understand their influence on chemical reactions and to improve reduction efficiency. This research represents a significant stride towards fostering sustainable practices in the realm of LIB cathode material recycling, addressing critical concerns related to resource management and environmental impact.

Received 5th March 2024
Accepted 8th July 2024

DOI: 10.1039/d4mr00018h

rsc.li/RSCMechanochem

Introduction

To address the increasing concentration of CO_2 in the atmosphere, a long standing transformation approaches is underway globally. A prominent shift is the transition of automotive vehicles towards electric vehicles (EVs) to mitigate the utilisation of fossil fuel combustion. To facilitate the electrification of these vehicles, lithium-ion batteries (LIBs) have emerged as the favoured energy storage technology owing to their exceptional performance characteristics.

As the lifespan of LIBs is currently estimated to be around ten years, a huge quantity of end-of-life (EoL) LIBs must be handled to ensure the complete recovery of strategic components and avoid soil, water and air pollution due to their disposal.[1,2] In fact, the worldwide EV inventory has undergone rapid expansion, starting from fewer than 1 600 000 units in 2015 to exceeding 17 400 000 units in 2021.[1] Moreover, metals used in LIB cathode materials (Co, Li, Mn, Ni, *etc.*) are considered strategic resources by several countries, and regulations concerning LIB recycling are evolving to ensure sustainable metal supplies for producing new LIBs.[3–5] Beyond resource scarcity and economic safety issues, recycling LIBs is beneficial in terms of energy consumption compared with the use of virgin resources.[6] Indeed, the metal extraction industry is known to be energy-intensive, and the large amounts of chemicals that can be released into the environment serve as additional sources of pollution. The production of cathode materials for LIBs using metal intermediates from LIB recycling has been proven to be twofold less energy-intensive than that using virgin raw materials.[7] Some studies have also highlighted that the production of cathode materials containing high-value metals, such as Ni and Co, from spent LIBs is economically more beneficial than using virgin materials.[3,8] This is because the average concentration of strategic metals in LIBs is 100- to 1000-fold higher than that in natural ores. For example, Co and Li contents are 5–20 wt% (based on the whole LIB) and 2–7 wt%, respectively.[9,10]

Recycling these metals while reducing secondary pollution caused by the current recycling processes is an urgent and important challenge.[11] The most common process for metal recovery is hydrometallurgy, either alone or in combination with pyrometallurgy.[2] It involves acid leaching of metal oxides followed by multiple separation and purification steps to selectively recover metals with sufficiently high purity for them

[a]*ICGM, Univ Montpellier, CNRS, ENSCM, Montpellier, France. E-mail: Laure.monconduit@umontpellier.fr*

[b]*Réseau sur le Stockage Electrochimique de l'Energie (RS2E), CNRS FR3459, Amiens, France*

[c]*SNAM, Avenue Jean Jaurès 12110, Viviez, France*

† Electronic supplementary information (ESI) available. See DOI: https://doi.org/10.1039/d4mr00018h

to be reused. This process is combined with pre-treatment steps, such as discharging, dismantling, crushing, pyrolysis, sieving, magnetic separation and other physical separation methods. Many combinations of these steps are possible with different arrangements according to the proprietary industrial routes. However, hydrometallurgical processes generate significant amounts of wastewater, are energy intensive and consume a large quantity of chemicals.[12,13]

While LIB recycling is expected to be the major source of battery elements by 2040 in the EU,[14] today, it is still in its infancy with a capacity of only 0.05–0.08 million tons per year (1.4 Mton per year by 2035).[15] Currently, the recycling rate of metals from LIBs is low at 22% for cobalt and less than 1% for Li; the recycling of the latter is not economically viable using conventional pyro and hydrometallurgical processes.[16] To date, a majority of spent LIBs on the market are those extracted from portable devices. However, with the fast development of the EV market, the flow of spent LIBs will increase significantly in the coming years (5 times). The capacity of the existing recycling plants is not sufficient to handle the increasing volume of spent LIBs. Therefore, the share of recycled LIBs is expected to decrease in the coming years.[2] Moreover, to achieve closed-loop recycling of cathode materials, metals have to be selectively recovered with high purity to meet the battery-grade specifications. The quality of recycled metals is closely linked to the method used for sorting the input feed, as well as the steps and the technologies employed in the recycling process because a great variety of LIB compositions exists in the market.[2,17]

Therefore, more advanced and efficient LIB recycling technologies are necessary to support the existing methods and fulfill the upcoming legislation targets towards limiting secondary pollution emissions. A technology that has garnered growing interest in the last decades is mechanochemistry (MC), which entails the activation of chemical reactions through mechanical energy. It usually works at room temperature and, most often, without a solvent. Therefore, it is energy-saving[18] and involves less reagent consumption.[19] These benefits are currently being explored for several processes of LIB recycling.[20] Different strategies have been proposed, such as MC-assisted leaching with organic acids,[21–25] ball milling as pre-treatment for the activation of the recycling feed,[26,27] reducing the cobalt and/or nickel species to activate leaching,[28–34] and solid-state chlorination to form water-soluble metal salts using organic wastes[35] or inorganic salts.[36–38] MC has also been investigated in other innovative processes, such as ammonia leaching[36] and the direct synthesis of new materials from spent cathodes.[39,40] Another promising MC-based technique is the direct recycling of cathode materials by relithiation, as no chemical separation steps are needed.[41] In this study, the strategy is to use MC for converting LCO to cobalt metal, which can then be selectively recovered by magnetic separation. This process has already been proposed by Dolokto *et al.* using aluminium as the reducing agent.[42,43] This work focuses on the influence of the ball milling parameters to elucidate the mechanisms of cobalt reduction and thereby optimise the energy consumption of this process. Understanding the mechanism is also beneficial to predicting scale-up issues. The magnetic separation step is not discussed here. The original cobalt quantification method was employed for quantifying metallic cobalt in the milled powder. Aluminium was chosen because of its low redox potential (-1.68 V *vs.* ESH for Al(III)/Al(0); 1.82 and -0.28 V *vs.* ESH for Co(III)/Co(II) and Co(II)/Co(0), respectively, at 25 °C in 1 M aqueous solution). Moreover, unlike Co, Al is currently not considered a critical resource and costs much less than Co. Lastly, Al is already present in spent LIBs as the cathode current collector and/or in the casing, which might render this process economically and environmentally attractive.

Experimental methods

Materials and methods

A Pulverisette 7 (Fritsch) planetary ball mill with ZrO_2 jars of 45 mL capacity was used. In order to establish the role of each investigated parameter, commercial $LiCoO_2$ powder (ABCR, 98%) was used as the model cathode material, and aluminium powder (Carl Roth, 99%) was employed as the reducing agent. LCO and Al powders were added to the ZrO_2 jar without any liquid. The impact of the reagent proportion (Al/LCO molar ratio) and ball milling parameters, such as milling time, rotation speed (300–500 rpm), ball diameter (5 and 10 mm), jar filling ratio, and power to ball mass ratio (P/B), were investigated. The milling process was stopped at selected reaction times, and a few milligrams of powder were extracted and analysed to monitor the reaction kinetics. Afterwards, the jars were closed, and milling was continued. To monitor the temperature of the reacting mixture, milling was briefly stopped at selected times, and the temperature of the external wall of the jar was measured with an infrared thermometer (Ebro® TFI 260).

Characterisation

The milled powder was analysed by X-ray diffraction (XRD) in reflection mode using a PANalytical Empyrean diffractometer equipped with Co K_α radiation ($K_{\alpha1}$ = 1.78901 Å and $K_{\alpha2}$ = 1.7929 Å) to identify the crystalline phases formed during ball milling. To determine the amount of Co metal obtained from the conversion of LCO, the magnetic moment of 10 to 30 mg of the ball-milled residues was measured using a SQUID magnetometer at 5000 Oe. As the amount of the analysed sample was small, the milled powder had to be homogeneous to get accurate results. The repeatability and accuracy of this method are described in ESI.† As the magnetic moment of cobalt metal (Co) at saturation is known (162 emu g^{-1} at 25 °C),[44,45] the mass of metallic Co in the sample was calculated according to eqn (1). SEM (Hitachi S4800) combined with an energy-dispersive X-ray analysis (EDX, Oxford Instruments X-Max SDD) was used for studying the morphology and particle composition of the milled powder.

$$m_{Co} = \frac{m_s \times M_s}{M_{Co}} \quad (1)$$

with m_s: sample mass (mg), M_s: measured magnetic moment of the sample at 5000 Oe (saturation) (emu g^{-1}), M_{Co}: theoretical magnetic moment of pure Co, M_{Co} = 162 emu g^{-1}.

From the LCO amount, the initial cobalt mass in the as-milled powder was determined. From this value, the cobalt fraction converted to Co metal was easily calculated using eqn (2):

$$X = \frac{m_{Co}}{m_s \times m\%_{Co,\,LCO} \times m\%_{LCO,\,milling\ residue}} \times 100 \qquad (2)$$

with $m\%_{Co\ (LCO)}$: mass ratio of cobalt in LCO, $m\%_{Co\ (LCO)} = 100 \times M_{Co}/M_{LCO} = 60\%$, $m_{\%LCO\ (milled\ p.)}$: mass ratio of LCO in the milled powder (LCO + Al), $m\%_{LCO\ (milled\ p.)} = m_{LCO}/(m_{LCO} + m_{Al})$

Results and discussion

Composition of the milling devices (jars and balls)

In a previous study, Dolotko *et al.*[43] used stainless steel (SS) jars and balls to achieve efficient reduction of LCO with Al. In this study, the reaction of LCO with Al during ball milling was first monitored as a function of milling time using either SS or zirconia jars and balls. The evolution of the XRD patterns of the residues at different milling times in the two systems is shown in Fig. 1. With the SS jar, LCO conversion was faster than that achieved with the ZrO_2 jar, as demonstrated by the main XRD peak of LCO at 22° (2θ). Crystalline LCO disappeared in less than 30 min in the case of SS, while it remained even after 1 h while using ZrO_2 in the same milling conditions. This faster kinetics of the reaction might be explained by the higher density of SS compared with ZrO_2 (Fritsch® data: $d_{ZrO_2} = 5.7$ g.cm^{-3}; $d_{SS} = 7.7$ g.cm^{-3}). Moreover, for the same number of balls with identical diameters, the impact energy was higher in the case of SS, leading to faster LCO conversion. The magnified XRD pattern in the region from 40° to 65° (Fig. 1c and d) showed an intense diffraction peak at around 52° (2θ) attributed to the formation of the cubic polymorph of Co metal, Co–Fe alloys and/or Fe metal.

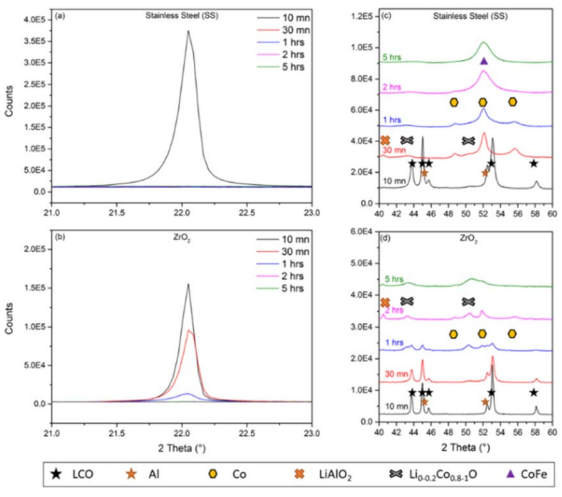

Fig. 1 XRD patterns of as-milled powder as a function of milling time (Al + LCO) in (a and c) stainless steel bowl and (b and d) ZrO_2 bowl. 500 rpm, 7 balls of 10 mm diameter, 1 g of powder (Al + LCO), mole ratio $n_{Al}/n_{Co} = 1$, milling/rest cycle = 15 min/10 min. Powder/ball mass ratio (P/B) = 0.04 (a and c) and 0.05 (b and d).

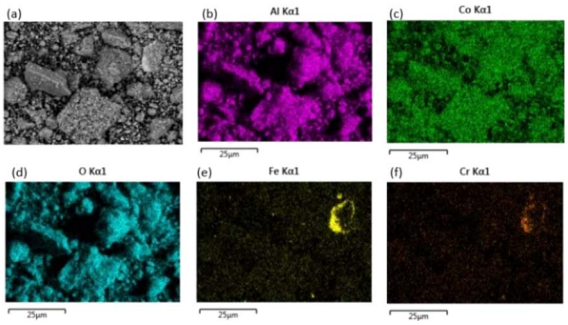

Fig. 2 SEM-EDX images of as-milled powder in the stainless steel jar after 5 h. Conditions: 500 rpm, 7 balls of 10 mm diameter, 1 g of powder (Al + LCO), mole ratio $n_{Al}/n_{Co} = 1$, and milling/rest cycle = 15 min/10 min.

The SEM-EDX analysis of the powder after 5 h of milling (Fig. 2) confirmed the presence of Fe and Cr as contaminants. The use of SS jar leads to extensive scratching and the consequent formation of ferromagnetic pollutants, which contaminate the cobalt. For this reason, ZrO_2 jar and balls were used subsequently in this study. It is worth noting that Dolotko *et al.*[43] used SS jars and balls to reduce cobalt with Al in their previous studies. However, even though they employed a 3D high-energy ball mill, they did not observe any Fe or CoFe alloy in the milled powder. The milling materials were not damaged in their case, as the milling duration was shorter (less than 3 h).

Al/LCO molar ratio (n_{Al}/n_{LCO})

The molar ratio of Al and Co is expected to be one of the key parameters regulating both reaction kinetics and the resulting products. Its influence was monitored at a constant milling time by XRD (Fig. 3). After 3 h of milling, complete conversion of LCO was observed by XRD for the $n_{Al}/n_{LCO} = 1.5$ mixture, with the formation of both AlCo and Co, whereas no structural modification was detected at $n_{Al}/n_{LCO} = 1.0$ (Fig. 3a and b). AlCo alloy formation is expected when an excess of Al is used, in line with the Al–Co phase diagram (Fig. S7†). For Al/LCO = 1.0, a weak XRD signal of metal cobalt was observed after 8 h (Fig. 3a). This is due to the addition of oxygen during sampling, which leads to Co(II) oxide formation. Adding an excess of Al

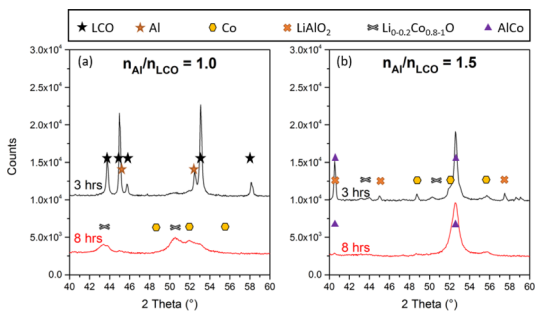

Fig. 3 XRD of as-milled powder as a function of the n_{Al}/n_{Co} ratio and milling time. Milling conditions: 500 rpm, 4 balls of 10 mm diameter, 1 g of powder (Al + LCO), milling/rest cycle = 15 min/10 min, P/B = 0.09, mole ratio $n_{Al}/n_{Co} = 1.0$ in (a) and 1.5 in (b).

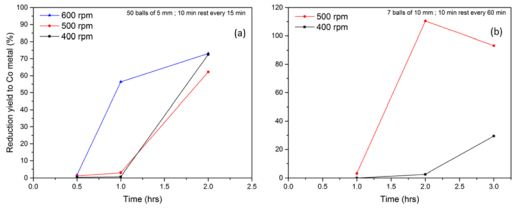

Fig. 4 Co conversion as a function of milling time (Al + LCO) in ZrO_2 bowls. Milling conditions: $n_{Al}/n_{Co} = 1.0$, 3 g of powder (Al + LCO), P/B = 0.15, (a) 50 balls of 5 mm diameter, milling/rest cycle = 15 min/10 min; (b) 7 balls of 10 mm diameter, and milling/rest cycle = 60 min/10 min.

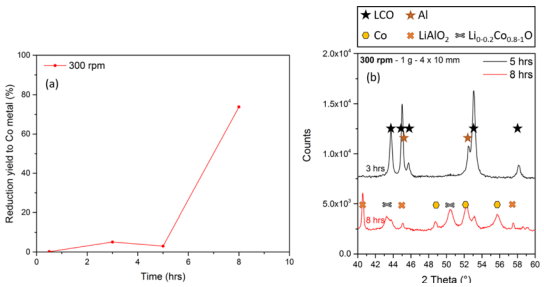

Fig. 5 (a) Co conversion rate as a function of milling time (Al + LCO). (b) XRD of as-milled powder as a function of milling time (Al + LCO) in ZrO_2 bowls. Milling conditions: ZrO_2 bowls, 4 balls of 10 mm diameter, 1 g of powder (Al + LCO), milling/rest cycle = 15 min/10 min, P/B = 0.08, and $n_{Al}/n_{LCO} = 1.0$.

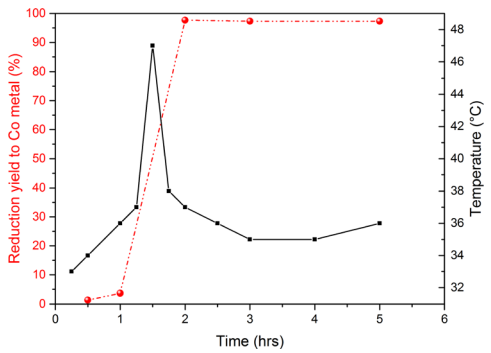

Fig. 6 Co conversion and bowl temperature as functions of milling time. Milling conditions: 7 balls of 10 mm diameter, 3 g of powder (Al + LCO), milling/rest cycle = 15 min/10 min, P/B = 0.15, and $n_{Al}/n_{Co} = 1.0$.

accelerates the reaction but mainly leads to the formation of the AlCo alloy, thus decreasing the selectivity of conversion to Co metal. Therefore, n_{Al}/n_{LCO} ratio is a key parameter that influences both reaction kinetics and the nature of the produced species.

As the kinetics was slower when an equimolar amount of Al was used, faster kinetics might be expected if more energy was brought to the system. To ascertain this possibility, milling speed, filling rate and the ball number and diameter were the parameters explored.

Rotation speed

In order to study the influence of rotation speed accurately, the ball-to-jar and ball-to-ball contacts have to be minimized so that the kinetic energy of the balls is transferred only to the milled powder. A solution to this is the use of a larger powder-to-ball mass ratio (P/B). This way, the balls will be always surrounded by the milled powder. For the experiments described in the following paragraph, a constant P/B ratio of 0.15 and a constant n_{Al}/n_{LCO} ratio of 1 were used.

Fig. 4a presents the LCO to Co metal conversion efficiency as a function of milling time based on the magnetometry analysis of the milled powders (3 g, Al + LCO) using 50 balls of 5 mm diameter and milling/rest cycle = 15 min/10 min. Under these conditions, about 60% of LCO was converted to Co metal after 1 h at 600 rpm, whereas no reaction occurred in the same milling time at 500 and 400 rpm. However, a similar conversion efficiency was observed when the milling time was extended to 2 h at both rotating speeds. Since no difference was observed between 400 and 500 rpm, these two conditions could be distinguished only by changing other parameters, such as the number and/or the size of the balls. For instance, the use of larger balls (7 balls of 10 mm diameter) and a shorter rest time (10 min rest every 60 min milling) allowed the differentiation of reaction kinetics between 400 and 500 rpm; complete conversion (110%) was observed after 2 h at 500 rpm, while no reaction (3%) occurred at 400 rpm (Fig. 4b). It is noteworthy that the conversion to Co metal exceeded 100% (500 rpm, 2 h) due to the uncertainty of the SQUID measurements, which were carried out with small quantities of samples (10–30 mg) in which controlling homogeneity is difficult.

In conclusion, increasing the rotation speed increases the kinetic energy of the balls and consequently the impact energy of the balls, as well as the distance browsed by the balls in the same period. Therefore, for a given milling time, more energy (determined by the rotation speed, the number and diameter of the balls, the rest time) will be released by the balls when the rotation speed is higher, and cobalt reduction will occur faster.[46]

The last experiment shows that the use of balls with a bigger size improves LCO reduction without increasing the rotation speed (which is costly). An attempt was then made to further decrease the rotation speed using balls of the same size. Fig. 5 shows the (a) Co metal quantification and (b) XRD patterns of a powder milled at 300 rpm. In this case, a P/B ratio of 0.08 was used to bring more energy to the powder and thereby facilitate the conversion reaction at such a low speed. The complete conversion of LCO occurred between 5 and 8 h, with a 70% selectivity to Co metal and the formation of CoO and $LiAlO_2$. This change was accompanied by a progressive temperature increase until the conversion reaction was triggered. Since the reaction is exothermic, the heat produced by the reaction might be transferred to the rest of the sample, producing a rapid local increase in temperature that suddenly accelerates LCO conversion.

To get better insights into this effect, the outside temperature of the bowl was monitored during milling. Fig. 6 shows the

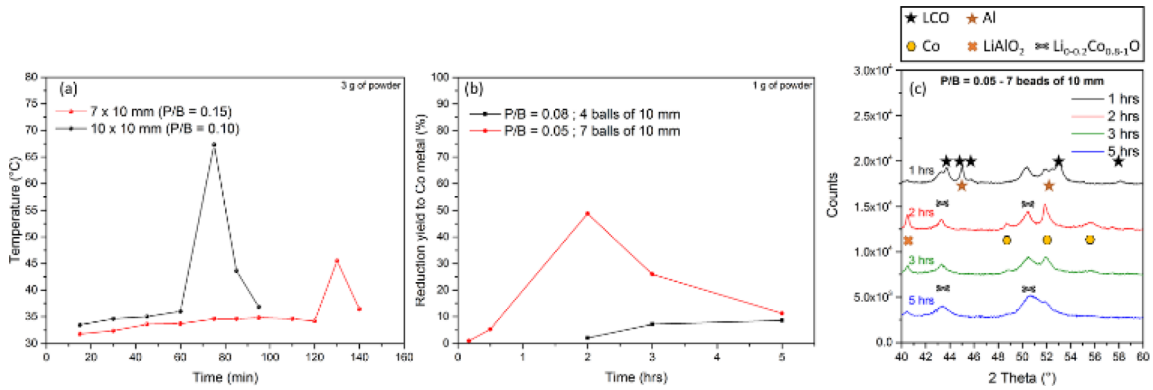

Fig. 7 Reaction kinetics study as a function of milling time (Al + LCO) in ZrO_2 bowls. Milling conditions: 10 mm balls, $n_{Al}/n_{LCO} = 1.0$, (a) 400 rpm, 3 g of powder (Al + LCO); (b and c) 500 rpm, milling/rest cycle = 15 min/10 min, 1 g of powder (Al + LCO). (a) Temperature monitoring. (b) Co conversion based on SQUID measurements. (c): XRD at 1, 2, 3 and 5 h of reaction with P/B = 0.05 and 7 balls of 10 mm diameter (the red line in (b)).

bowl temperature evolution and the amount of cobalt obtained from LCO conversion as functions of milling time. The exothermic peak observed between 2 and 3 hours corresponds to LCO reduction. The influence of the exothermicity of LCO reduction is discussed in detail later in the article (*vide infra*).

Powder/ball mass ratio (P/B)

Two strategies were adopted to investigate the influence of the P/B ratio on the reaction kinetics: (i) varying the ball mass while keeping the powder mass constant; (ii) varying the powder mass while keeping the ball mass constant.

Fig. 7a shows the temperature evolution of the bowl at two different P/B ratios. The powder mass was kept constant at 3 g, and the number of 10 mm balls was varied from 7 to 10 balls corresponding to the P/B ratios of 0.15 and 0.10, respectively. Temperature monitoring evidenced a faster reaction when a higher number of balls was used, with an exothermic peak observed after 75 min of reaction with 10 balls, while it appeared only after 130 min with 7 balls (Fig. 7a). A similar behaviour was observed while studying the magnetic moment of the milled powder to determine the cobalt reduction efficiency, as shown in Fig. 7b. A reduction yield of 50% was measured after 2 h of milling with 7 balls, whereas no reaction was observed with 5 balls in the same reaction time. In conclusion, the lower the number of balls, the slower the reaction as there are less contact points and less friction to activate the reaction.

As seen in Fig. 7b, a conversion drop occurred after 2 h of milling with 7 balls. This phenomenon is probably due to the oxidation of the Co metal by its reaction with the oxygen brought into the jar when it was opened for sampling. The formation of CoO during milling was confirmed by XRD analysis (Fig. 7c). Furthermore, XRD also detected the progressive consumption of LCO and Al, confirming the partial reduction of cobalt after 1 h. After 2 h, no LCO and Al were detected, while hexagonal Co metal and $LiAlO_2$ were formed. With further milling, the peaks of Co decreased in intensity and that of CoO prevailed. Therefore, limiting sampling and air exposure during the milling process is fundamental for studying the Co reduction more accurately. Thus, temperature monitoring is a better way to study the reaction kinetics as the bowl remains closed.

As mentioned above, experiments were also carried out with a constant number of balls (50 of 5 mm diameter) by varying the mass of the powder (3 and 5 g) under the same milling conditions (500 rpm, milling/rest time = 15 min/10 min). However, no difference was observed by XRD between these two experiments. LCO and Al disappeared completely after 1 h, and the reaction was too fast to differentiate between the two conditions. The only difference was in the morphology of the obtained powder (Fig. S8†); for a higher amount of powder (5 g), sheet-like millimeter-size agglomerates were observed, whereas for 3 g, the milled powder was more homogeneous. As the heat released is proportional to the amount of reagent, with 5 g, the heat released was higher than that obtained with 3 g, and therefore, the reaction was more intense with a fast cobalt reduction reaction, leading to Co metal agglomerates.

The temperature of the jars was recorded as a function of milling time using four different amounts of powder (1, 2, 3 and 5 g). The results shown in Fig. 8 highlight a remarkable difference in reaction kinetics, with an exothermic peak at 40 min (40

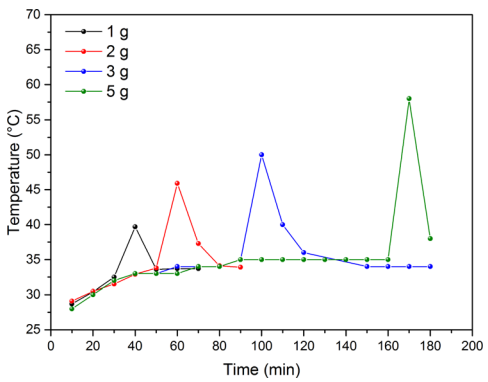

Fig. 8 External bowl temperature as a function of milling time with varying powder mass. Milling conditions: 450 rpm, 7 × 10 mm balls, no rest time, and $n_{Al}/n_{Co} = 1.0$.

°C), 60 min (46 °C), 100 min (50 °C) and 170 min (58 °C) for 1, 2, 3 and 5 g, respectively. Reaction activation was the fastest at the lowest P/B ratio. Nevertheless, even though the reaction with the highest powder mass was slower, the temperature build-up was higher. This phenomenon is due to the high exothermicity of the LCO reduction reaction using Al metal to produce $LiAlO_2$ and Co metal (−510.5 kJ mol^{-1}, see ESI† for additional details).

Influence of ball diameter

The influence of the diameter of the balls used for milling was also investigated at a constant P/B ratio. Two experiments were carried out with 5 and 10 mm balls (fixed conditions: 500 rpm, 5 g of powder, $n_{Al}/n_{LCO} = 1.0$, P/B = 0.32, milling/rest time cycles = 15 min/10 min). After 3 h, 55% and 5% cobalt reduction efficiency were measured by SQUID magnetometry for the 5 and 10 mm balls, respectively. Therefore, 5 mm balls are enough to reach the activation energy required to reduce cobalt from LCO using Al. As larger balls are heavier, they bring a higher impact energy, which would help activate the reaction.[47] However, the contact surface of the balls with the powder should also be considered. In fact, although small balls individually have a lower impact energy, their total contact surface is larger than that of fewer big balls. Therefore, for the same mass of balls, if the ball diameter is large enough to activate the reaction, smaller balls ensure greater contact with the reagents, leading to the simultaneous initiation of the reaction at a higher number of points.

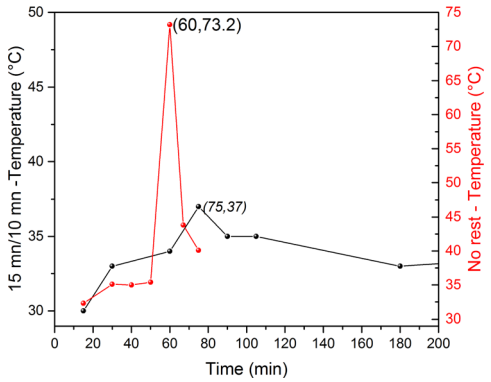

Fig. 9 Influence of rest time during milling cycles. Milling bowl temperature as a function of milling/rest time: the red curve represents continuous milling without rest time, and the black curve represents cycles of 15 minutes of milling followed by 10 minutes of rest. Milling conditions: Al/LCO = 1.0, 7 × 10 mm balls, P/B = 0.15, and 500 rpm.

Rest time between milling cycles and exothermicity

As LCO reduction is exothermic, energy dissipation will affect the reaction kinetics considerably. One of the parameters that affect energy dissipation the most is the relative duration of milling and rest. During mechanochemical reactions, rest time is used and prescribed to limit temperature build-up and particle agglomeration. However, for LCO reduction, temperature build-up is needed for the activation of the reaction. For this reason, the influence of the milling and rest durations was studied in order to limit heat dissipation.

The effect of milling time was studied by SQUID magnetometry while all the other parameters were kept constant. With a lower rest time of 10 min for every 30 min of milling, the reduction yield improved quickly to around 50% after 1 h, while no metallic cobalt was measured by this time with 10 min of rest time for every 15 min of milling (fixed conditions: 500 rpm, 3 g of powder, $n_{Al}/n_{Co} = 1.0$, P/B = 0.15, 50 × 5 mm balls). The reduction yield of Co metal was only measured after 2 h of milling (around 55%). These results show that temperature build-up within the cell is an important parameter influencing the conversion of LCO to Co metal.

These results were confirmed by the comparison of the external wall temperatures of the milling jar, as shown in Fig. 9, between two different milling experiments carried out at 500 rpm with 7 balls of 10 mm diameter, 3 g of powder and a P/B ratio of 0.15. A sudden and steep increase in temperature was observed after 60 min of continuous milling without rest,

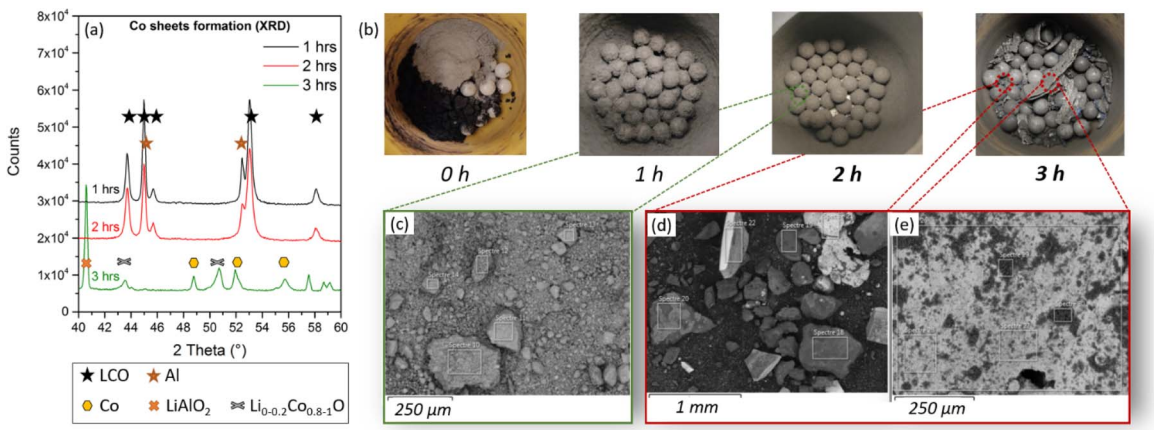

Fig. 10 (a) XRD patterns of the as-milled powder. (b) Images of the as-milled powder at different milling times. Milling conditions: 500 rpm, powder mass (Al + LCO) = 5 g, Al/LCO = 1.0, milling/rest cycle = 15 min/10 min, P/B = 0.33, 37 balls of 5 mm diameter. SEM pictures of the milled powder after milling for (c) 2 h and (d and e) 3 h. (d) Image of the milled powder and (e) the sheet-like particle.

whereas the increase in temperature was lower and observed only after 75 min when a rest of 10 min was applied after every 15 min of milling. In summary, the application of regular rest times during milling is a crucial parameter as it allows heat dissipation and slows down the reaction, confirming that reaction activation is not only dependent on the milling time but also on the temperature build-up in the system. This temperature increase helps in reaching the activation threshold, thereby triggering LCO reduction, which then produces more heat and leads to a rapid reaction in the entire mass of powder. These results confirm the results presented in Fig. 6 (*vide supra*), which shows that the LCO conversion is strongly correlated with the reaction temperature within the jar.

The control of temperature build-up by changing the milling parameters, however, is also important to obtain a homogeneous powder and to avoid damage to the jar and the balls. For example, before milling at 500 rpm with milling/rest cycles of 15/10 min, no structural change was observed by XRD (Fig. 10a). This means that no reaction occurred, and the composition of the milled powder is homogeneous in terms of composition, even if it appeared agglomerated, as observed through SEM (Fig. 10c, S8, S9, Tables S1, S2 and S3†). After 3 h of milling, the reaction occurred suddenly, producing sheet-like particles measuring a few centimetres. Their SEM-EDX analysis (Fig. 10e) revealed that the sheets consisted of Co metal covered on the surface by small particles enriched in Al. Such large Co sheets could damage the balls during milling, as shown in Fig. 10d, and some ZrO_2 particles were also detected.

In order to avoid damage to both the milling jar and the balls, temperature build-up and the milling energy have to be controlled. With a shorter rest time, the reaction will be more violent, and more resistant (bigger) balls should be used to decrease the number of reaction activation sites, as well as the temperature build-up. Regarding the milling speed, a compromise had to be made between energy consumption and the processing time for LCO reduction. For example, at 500 rpm, with 7 balls of 10 mm diameter, 3 g of powder and 15/10 min milling/rest cycles, LCO conversion to Co metal was possible after 2 h (Fig. 11). Nevertheless, to limit energy consumption,

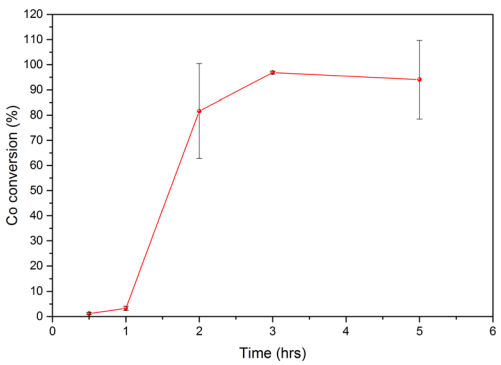

Fig. 11 Co conversion rate as a function of milling time. Milling conditions: 500 rpm, 3 g of powder (Al + LCO), $n_{Al}/n_{Co} = 1.0$, P/B = 0.15, 7 × 10 mm balls. These results report the average of 3 experiments performed in the same conditions.

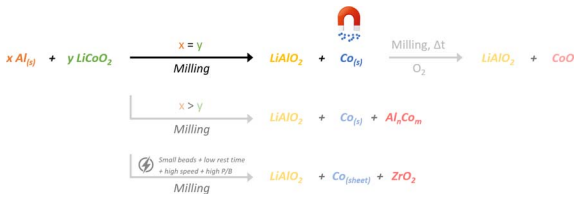

Fig. 12 Different reaction pathways as functions of the applied milling conditions.

the reaction time can be still decreased by removing the rest time and using a smaller number of balls and/or a slower rotation speed if the reaction is too violent. Another strategy would be to decrease the amount of powder to limit heat release. In this case, however, a smaller amount of cathode material will be treated and the energy required per mass of powder will be higher.

A summary of the different reaction pathways as a function of the milling conditions is shown in Fig. 12. Notably, the renewal of the oxygenated atmosphere caused by powder sampling for the characterisation of the intermediate states impacts the formation of Co metal. The maximum production of Co metal requires no air exposure during milling and equimolar amounts of LCO and Al. LCO conversion is faster for high milling energy but the high temperature increase may damage the milling materials. Therefore, milling speed, rest time, powder amount, and the number of balls have to be balanced to limit temperature increase and avoid ZrO_2 pollution from the ball mill. The as-formed $LiAlO_2$ side product can be leached for Li^+ recovery.[48,49] This material can be easily valorised to produce coatings for cathode materials towards improving their electrochemical performance.[50–52]

The triggering mechanism of the reaction is still under investigation. XRD refinement of the milled powder sample before LCO conversion was performed to study the evolution of lattice parameters. No significant change in the lattice parameters of LCO and Al was observed with variation in milling time (Fig. S11†). Further work is under process, such as the study of the amorphisation of the reagents, which is supposed to be correlated with the triggering of cobalt reduction in addition to temperature build-up to reach the activation energy threshold.

Conclusion

A mechanochemical process assisted by magnetic extraction was used to reduce $LiCoO_2$ using Al to obtain cobalt. A systematic study of the different ball milling parameters (number of balls, powder/ball mass ratio, duration of milling, and milling/rest ratio) was carried out for process optimisation. LCO reduction was found to take place with a fast increase in jar temperature caused by the release of heat, evidencing the exothermicity of the reaction. This energy release affects the kinetics of LCO conversion, as well as the homogeneity and the integrity of the milled powder. As the rate of conversion to Co metal is directly related to the energy supplied to the system, very high energy leads to the formation of large Co metal

shavings with simultaneous damage to the milling jar and balls, leading to ZrO_2 contamination in the milled powder. In conclusion, a complete reduction of cobalt can be reached after 2 h of milling at 500 rpm, and this reaction time can be decreased by reducing the rest time during milling. Considering the extension of this process to relevant industrial conditions with larger amounts of LCO, the inhomogeneity of the milled powder will be less of an issue as larger balls will probably have to be used. Further optimisation of parameters is required for scaling up this process. In particular, the ball milling process should be optimised to deal with larger volumes of cathode materials. A temperature sensor inside the milling jars would however be useful to ensure safety, and the process of milling can be stopped if the temperature rises beyond a certain limit. Finally, even if the Al content from EoL LIBs is lower than that of Co, Al scrap from metallurgical plants might be used as a cheap reagent.

Conflicts of interest

There are no conflicts to declare.

Acknowledgements

The authors would like to acknowledge SNAM and the Région Occitanie for the financial support. The authors gratefully acknowledge the French National Research Agency (project Labex STORE-EX, ANR-10-LABX-76-01) for financial support.

Notes and references

1 S. Jin, D. Mu, Z. Lu, R. Li, Z. Liu, Y. Wang, S. Tian and C. Dai, *J. Clean. Prod.*, 2022, **340**, 130535.
2 D. Latini, M. Vaccari, M. Lagnoni, M. Orefice, F. Mathieux, J. Huisman, L. Tognotti and A. Bertei, *J. Power Sources*, 2022, **546**, 231979.
3 J. Neumann, M. Petranikova, M. Meeus, J. D. Gamarra, R. Younesi, M. Winter and S. Nowak, *Adv. Energy Mater.*, 2022, **12**, 2102917.
4 M. M. Cerrillo-Gonzalez, M. Villen-Guzman, C. Vereda-Alonso, J. M. Rodriguez-Maroto and J. M. Paz-Garcia, *Chemosphere*, 2022, **287**, 132020.
5 European Parliament Adopted Text, *Batteries and Waste Batteries-P9_TA, (2023)0237*, 2023.
6 T. Or, S. W. D. Gourley, K. Kaliyappan, A. Yu and Z. Chen, *Carbon Energy*, 2020, **2**, 6–43.
7 L. Gaines, J. Sullivan, A. Burnham and I. Belharouak, *Transp. Res. Rec.*, 2011, 57–65.
8 E. Fan, L. Li, Z. Wang, J. Lin, Y. Huang, Y. Yao, R. Chen and F. Wu, *Chem. Rev.*, 2020, **120**, 7020–7063.
9 S. M. Shin, N. H. Kim, J. S. Sohn, D. H. Yang and Y. H. Kim, *Hydrometallurgy*, 2005, **79**, 172–181.
10 B. Huang, Z. Pan, X. Su and L. An, *J. Power Sources*, 2018, **399**, 274–286.
11 J. Lin, X. Zhang, L. Cai, E. Fan, S. Wu, S. Ma, F. Wu, R. Chen and L. Li, *Adv. Energy Sustainability Res.*, 2022, **3**, 2100153.
12 J. J. Roy, S. Rarotra, V. Krikstolaityte, K. W. Zhuoran, Y. D. Cindy, X. Y. Tan, M. Carboni, D. Meyer, Q. Yan and M. Srinivasan, *Adv. Mater.*, 2022, **34**, 2103346.
13 R. Golmohammadzadeh, F. Faraji and F. Rashchi, *Resour. Conserv. Recycl.*, 2018, **136**, 418–435.
14 L. Gregoir and K. Van Acker, *Metals for Clean Energy: Pathways to solving Europe's raw materials challenges*, Eurometaux and KU Leuven, 2022.
15 S. W.-Kern, E. Gerold, T. Nigl, A. Jandric, M. Altendorfer, B. Rutrecht, S. Scherhaufer, H. Raupenstrauch, R. Pomberger, H. Antrekowitsch and F. Part, *Waste Manag.*, 2022, **138**, 125–139.
16 Z. Takacova, D. Orac, J. Klimko and A. Miskufova, *Mater.*, 2023, **16**, 4264.
17 W. Yu, Y. Guo, S. Xu, Y. Yang, Y. Zhao and J. Zhang, *Energy Storage Mater.*, 2023, **54**, 172–220.
18 S. Babanejad, H. Ahmed, C. Andersson and E. P. Heikkinen, *J. Sustain. Met.*, 2023, **9**, 522–536.
19 M. Baláž, *Environmental Mechanochemistry*, Springer International Publishing, Cham, 2021.
20 M. Wang, K. Liu, J. Yu, C.-C. Zhang, Z. Zhang and Q. Tan, *Circ. Econ.*, 2022, 100012.
21 L. Cai, J. Lin, E. Fan, F. Wu, R. Chen and L. Li, *ACS Sustain. Chem. Eng.*, 2022, **10**, 10649–10657.
22 M.-M. Wang, C.-C. Zhang and F.-S. Zhang, *Waste Manag.*, 2016, **51**, 239–244.
23 E. Fan, L. Li, X. Zhang, Y. Bian, Q. Xue, J. Wu, F. Wu and R. Chen, *ACS Sustain. Chem. Eng.*, 2018, **6**, 11029–11035.
24 L. Li, Y. Bian, X. Zhang, Y. Yao, Q. Xue, E. Fan, F. Wu and R. Chen, *Waste Manag.*, 2019, **85**, 437–444.
25 Z. Liang, G. Peng, J. Hu, H. Hou, C. Cai, X. Yang, S. Chen, L. Liu, S. Liang, K. Xiao, S. Yuan, S. Zhou and J. Yang, *Waste Manag.*, 2022, **150**, 290–300.
26 Y. Yang, X. Zheng, H. Cao, C. Zhao, X. Lin, P. Ning, Y. Zhang, W. Jin and Z. Sun, *ACS Sustain. Chem. Eng.*, 2017, **5**, 9972–9980.
27 Q. Zhang, J. Lu, F. Saito, C. Nagata and Y. Ito, *Adv. Powder Technol.*, 2000, **11**, 353–359.
28 Y. Guo, Y. Li, X. Lou, J. Guan, Y. Li, X. Mai, H. Liu, C. X. Zhao, N. Wang, C. Yan, G. Gao, H. Yuan, J. Dai, R. Su and Z. Guo, *J. Mater. Sci.*, 2018, **53**, 13790–13800.
29 M. Wang, Q. Tan and J. Li, *Environ. Sci. Technol.*, 2018, **52**, 13136–13143.
30 J. Xie, K. Huang, Z. Nie, W. Yuan, X. Wang, Q. Song, X. Zhang, C. Zhang, J. Wang and J. C. Crittenden, *Resour. Conserv. Recycl.*, 2021, **168**, 105261.
31 Y. Jiang, X. Chen, S. Yan, Y. Ou and T. Zhou, *Green Chem.*, 2022, **24**, 5987–5997.
32 J. Guan, Y. Li, Y. Guo, R. Su, G. Gao, H. Song, H. Yuan, B. Liang and Z. Guo, *ACS Sustain. Chem. Eng.*, 2017, **5**, 1026–1032.
33 L. QU, Y. HE, Y. FU, W. XIE, C. YE, Q. LU, J. LI, J. LI and Z. PANG, *Trans. Nonferrous Met. Soc. China*, 2022, **32**, 1325–1335.
34 J. Yang, L. Jiang, F. Liu, M. Jia and Y. Lai, *Trans. Nonferrous Met. Soc. China*, 2020, **30**, 2256–2264.

35 S. Saeki, J. Lee, Q. Zhang and F. Saito, *Int. J. Miner. Process.*, 2004, **74**, 373–378.
36 S. Zhang, C. Zhang, X. Zhang and E. Ma, *ACS Sustain. Chem. Eng.*, 2022, **10**(17), 5611–5620.
37 M. Wang, Q. Tan, L. Liu and J. Li, *J. Clean. Prod.*, 2021, **279**, 123612.
38 K. Liu, Q. Tan, L. Liu and J. Li, *Environ. Sci. Technol.*, 2019, **53**, 9781–9788.
39 S. Dang, P. Zhou, P. Shi, Y. Min and Q. Xu, *ACS Sustain. Chem. Eng.*, 2021, **9**, 15375–15385.
40 Y. Yang, H. Yang, H. Cao, Z. Wang, C. Liu, Y. Sun, H. Zhao, Y. Zhang and Z. Sun, *J. Clean. Prod.*, 2019, **236**, 117576.
41 X. Meng, J. Hao, H. Cao, X. Lin, P. Ning, X. Zheng, J. Chang, X. Zhang, B. Wang and Z. Sun, *Waste Manag.*, 2019, **84**, 54–63.
42 O. Dolotko, N. Gehrke, T. Malliaridou, R. Sieweck, L. Herrmann, B. Hunzinger, M. Knapp and H. Ehrenberg, *Commun. Chem.*, 2023, **6**, 49.
43 O. Dolotko, I. Z. Hlova, Y. Mudryk, S. Gupta and V. P. Balema, *J. Alloys Compd.*, 2020, **824**, 153876.
44 J. I. Schwerdt, G. F. Goya, M. P. Calatayud, C. B. Hereñú, P. C. Reggiani and R. G. Goya, *Curr. Gene Ther.*, 2012, **12**, 116–126.
45 U. Ritter, P. Scharff, G. E. Grechnev, V. A. Desnenko, A. V. Fedorchenko, A. S. Panfilov, Y. I. Prylutskyy and Y. A. Kolesnichenko, *Carbon*, 2011, **49**, 4443–4448.
46 C. Brisan and M. Hiller, *Rom*, 2002, **14**, 11–20.
47 H. X. Kho, S. Bae, S. Bae, B.-W. Kim and J. S. Kim, *J. Kor. Powder Metall. Inst.*, 2014, **21**, 155–164.
48 J. Shin, J. M. Jeong, J. B. Lee, N. S. Heo, H. Kwon, Y. H. Kim and T. Ryu, *Hydrometallurgy*, 2023, 215.
49 Y. Kim, Y. Han, S. Kim and H. S. Jeon, *Process Saf. Environ. Prot.*, 2021, **148**, 765–774.
50 C. Zou, L. Yang, Z. Zang, X. Tao, L. Yi, X. Chen, X. Liu, X. Zhang and X. Wang, *Ceram. Int.*, 2023, **49**, 443–449.
51 X. He, H. Luo, K. Yong, M. Yao and Y. Zhang, *J. Energy Storage*, 2023, **70**, 107872.
52 Y. Duan, D. C. Sorescu, W. Jiang and D. J. Senor, *J. Nucl. Mater.*, 2020, **530**, 151963.